

¹ Study of neutrino-nucleus interaction at around 1 GeV using
² a 3D grid-structure neutrino detector, WAGASCI at J-PARC
³ neutrino monitor hall

⁴ A. Bonnemaison, R. Cornat, L. Domine, O. Drapier, O. Ferreira, F. Gastaldi,
⁵ M. Gonin, J. Imber, M. Licciardi, F. Magniette, T. Mueller, L. Vignoli, and O. Volcy

⁶ *Ecole Polytechnique, IN2P3-CNRS, Laboratoire Leprince-Ringuet, Palaiseau,
7 France*

⁸ S. Cao and T. Kobayashi

⁹ *High Energy Accelerator Research Organization (KEK), Tsukuba, Ibaraki, Japan*

¹⁰ M. Khabibullin, A. Khotjantsev, A. Kostin, Y. Kudenko, A. Mefodiev, O. Mineev,
¹¹ S. Suvorov, and N. Yershov

¹² *Institute for Nuclear Research of the Russian Academy of Sciences, Moscow, Russia*

¹³ B. Quilain

¹⁴ *Kavli Institute for the Physics and Mathematics of the Universe (WPI), The
15 University of Tokyo Institutes for Advanced Study, University of Tokyo, Kashiwa,
16 Chiba, Japan*

¹⁷ T. Hayashino, A. Hiramoto, A.K. Ichikawa, K. Nakamura, T. Nakaya, K Yasutome,
¹⁸ and K. Yoshida

¹⁹ *Kyoto University, Department of Physics, Kyoto, Japan*

²⁰ Y. Azuma, J. Harada, T. Inoue, K. Kin, N. Kukita, S. Tanaka, Y. Seiya,
²¹ K. Wakamatsu, and K. Yamamoto

²² *Osaka City University, Department of Physics, Osaka, Japan*

23 A. Blondel, F. Cadoux, Y. Karadzhov, Y. Favere, E. Noah, L. Nicola, S. Parsa, and
24 M. Rayner

25 *University of Geneva, Section de Physique, DPNC, Geneva, Switzerland*

26 N. Chikuma, F. Hosomi, T. Koga, R. Tamura, and M. Yokoyama

27 *University of Tokyo, Department of Physics, Tokyo, Japan*

28 Y. Hayato

29 *University of Tokyo, Institute for Cosmic Ray Research, Kamioka Observatory,
30 Kamioka, Japan*

31 Y. Asada, K. Matsushita, A. Minamino, K. Okamoto, and D. Yamaguchi

32 *Yokoyama National University, Faculty of Engineering, Yokoyama, Japan*

33 December 5, 2017

34 **1 Introduction**

35 The understanding of neutrino-nucleus interactions in the 1 GeV energy region is critical
36 for the success of accelerator-based neutrino oscillation experiments such as the T2K exper-
37 iment. Complicated multi-body effects of nuclei render this understanding difficult. The
38 T2K near detectors have been measuring these and significant progress has been achieved.
39 However, the understanding is still limited. One of the big factors preventing from full
40 understanding is the non-monochromatic neutrino beam spectrum. Measurements with
41 different but some overlapping beam spectra would greatly benefit to resolve the contri-
42 bution from different neutrino energies. We, the Wagasci collaboration, proposes to study
43 the neutrino-nucleus interaction at the B2 floor of the neutrino monitor building, where
44 different neutrino spectra can be obtained due to the different off-axis position. Our experi-
45 mental setup contains 3D grid-structure plastic-scintillator detectors filled with water as the
46 neutrino interaction target (Wagasci modules), two side- and one downstream- muon range
47 detectors(MRD's). The 3D grid-structure and side-MRD's allows a measuremen of wider-
48 angle scattering than the T2K off-axis near detector (ND280). High water to scitillator
49 material ratio enables the measurement of the neutrino interaction on water, which is higly
50 desired for the T2K experiment because it's far detector, Super-Kamiokande, is composed

51 of water. The MRD's consist of plastic scintillators and iron plates. The downstream-
52 MRD, so called the Baby MIND detector, is also work as a magnet and provides the
53 charge identification capability. The charge identification is essentially important to select
54 antineutrino events in the antineutrino beam because contamination of the neutrino events
55 is as high as 30%. Most of the detectors has been already constructed and commissioned as
56 the J-PARC T59 experiment. Therefore, the collaboration will be ready to proceed to the
57 physics data daking for the T2K beam time in January 2019. We will provide the cross sec-
58 tions of the charged current neutrino and antineutrino interactions on water with slightly
59 higher neutrino energy than T2K ND280 with wide angler acceptance. When combined
60 with ND280 measurements, our measurement would greatly improve the understanding of
61 the neutrino interaction at around 1 GeV and contribute to reduce the most significant
62 uncertainty of the T2K experiment.

63 **2 Experimental Setup**

64 Figure. 1 shows a schematic view of the entire set of detectors. A central detector, Wagasci
65 modules, consists of 3D grid-structure plastic-scintillator detectors filled with water as the
66 neturino interaction target. They are surrounded by two side- and one downstream- muon
67 range detectors(MRD's) The MRD's are used to select muon tracks from the charged-
68 current (CC) interactions and to reject short tracks caused by neutral particles that orig-
69 inate mainly from neutrino interactions in material surrounding the central detector, like
70 the walls of the detector hall, neutrons and gammas, or neutral-current (NC) interactions.
71 The muon momentum can be reconstructed from its range inside the detector. The MRD's
72 consist of plastic scintillators and iron plates. In addition, eaco of the iron plates of the
73 downstream-MRD, so called the Baby MIND detector, is wound by a coil and can be
74 magnetized. It provide the charge selection capability.

75 For all detectors, scintillation light in the scintillator bar is collected and transported
76 to a photodetector with a wavelength shifting fiber (WLS fiber). The light is read out by
77 a photodetector, Multi-Pixel Photon Counter (MPPC), attached to one end of the WLS
78 fiber. The signal from the MPPC is read out by the dedicated electronics developed for the
79 test experiment to enable bunch separation in the beam spill. The readout electronics is
80 triggered using the beam-timing signal from MR to synchronize to the beam. The beam-
81 timing signal is branched from those for T2K, and will not cause any effect on the T2K
82 data taking.

83 T2K adopted the off-axis beam method, in which the neutrino beam is intentionally
84 directed 2.5 degrees away from SK producing a narrowband ν_μ beam. The off-axis near
85 detector, ND280, is installed towards the SK direction in the B1 floor of the near detector
86 hall of the J-PARC neutrino beam-line. We propose to install our detector in the B2 floor
87 of the near detector hall, where the off-axis angle is similar but slightly different. The
88 candidate detector position in the B2 floor is shown in Fig. 2. The expected neutrino

tmp.pdf

Figure 1: Schematic view of entire sets of detectors.

89 energy spectrum at the candidate position is shown in Fig. 3.

90 **2.1 Wagasci module**

91 The dimension of the central detector is 100cm \times 100cm in the x and y directions and
92 200cm along the beam direction. The total water and hydrocarbon masses serving as
93 neutrino targets are \sim 1 ton each. Inside the central detector, plastic scintillator bars are
94 aligned as a 3D grid-like structure, shown in Fig. 4, and spaces in the structure are filled
95 with the neutrino target materials, water and hydrocarbon. When neutrinos interact with
96 hydrogen, oxygen or carbon, in water and hydrocarbon, charged particles are generated.
97 Neutrino interactions are identified by detecting tracks of charged particles through plastic
98 scintillation bars. Thanks to the 3 D grid-like structure of the scintillator bars, the central
99 detector has 4π angular acceptance for charged particles. Furthermore, adopting a 2.5cm
100 grid spacing, short tracks originated from protons and charged pions can be reconstructed
101 with high efficiency. Thin plastic scintillator bars (thickness \sim 0.3cm) will be used for the
102 central detector to reduce the mass ratio of scintillator bars to neutrino target materials,
103 because neutrino interactions in the scintillator bars are a background for the cross section
104 measurements. Scintillator bars whose dimensions are 2.5cm x 0.3cm x 100cm will be used
105 for the central detector. The total number of channels in the central detector is 12880.

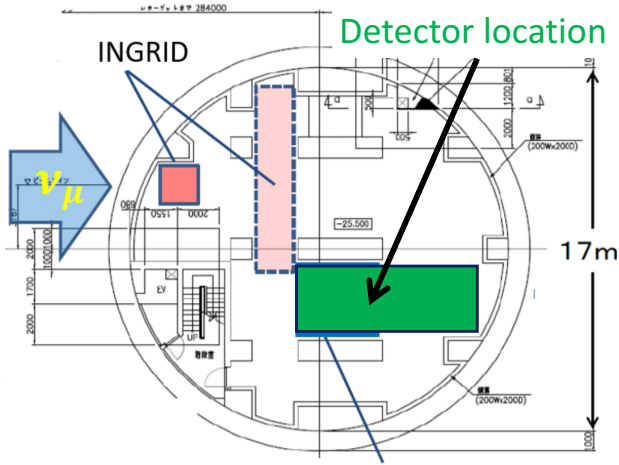


Figure 2: Candidate detector position in the B2 floor of the near detector hall.

¹⁰⁶ **2.2 Baby MIND**

¹⁰⁷ **2.3 Side muon range detector**

¹⁰⁸ Two Side-MRD modules will be constructed by the end of January 2018. Each Side-MRD
¹⁰⁹ module is composed of iron plates and scintillator bars for tracking secondary particles
¹¹⁰ from neutrino interactions. Support structure of the Side-MRD module mainly consists of
¹¹¹ 11 steel plates of which dimensions are $1800 \times 1610 \times 30$ mm³, is sized as $2236 \times 1630 \times$
¹¹² 975 mm³ as shown in Fig. 5, and weights ~ 8.5 ton. Scintillator bars were produced
¹¹³ by Uniplast company in Vladimir, Russia. Each bar is polystyrene based and made by
¹¹⁴ extrusion technology with scintillating composition of 1.5% PTP and 0.01% POPOP. Then
¹¹⁵ each bar's surface is etched by a chemical agent to form a white diffuse layer. The usage
¹¹⁶ of this method gives almost ideal contact between the scintillator and the reflector which
¹¹⁷ allows us to gain in light yield up to 50% compared to clear scintillator. 80 scintillator bars
¹¹⁸ are installed in one Side-MRD module, and each scintillator bar is sized as $1800 \times 200 \times 7$
¹¹⁹ mm³ including reflector part. Scintillation light is collected by wave length shifting fibers,
¹²⁰ Y-11 (S type) with a diameter of 1.0 mm produced by Kuraray. The fiber is glued by
¹²¹ optical cement EJ-500 in a S-shape groove on the surface of the scintillator bar as shown
¹²² in Fig. 6. Using this technique allows us to uniform light collection over scintillator's
¹²³ surfaces. Two optical connectors as shown in Fig. 7 are attached to either end of the fiber,
¹²⁴ and scintillation light is lead to two MPPCs, S13081-050CS(X1), produced at Hamamatsu
¹²⁵ Photonics. Optical connector of such type (so-called Baby-mind type of optical connector)
¹²⁶ consists of two parts (see Fig. 7): a) a MPPC cover and b) a ferrule. Ferrule b) is fixed in

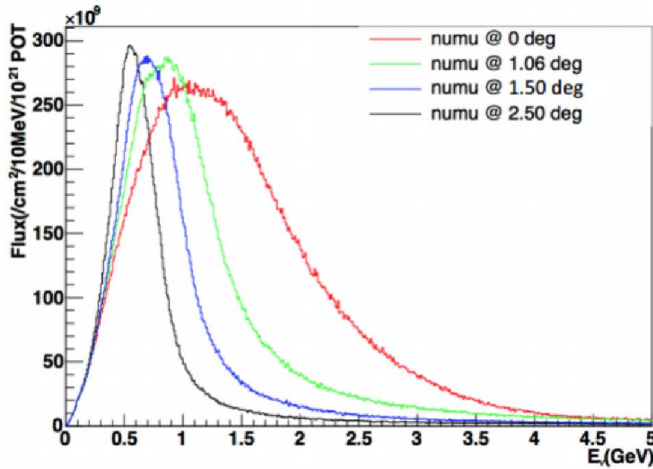


Figure 3: Neutrino energy spectrum at the candidate detector position(red). The spectrum at the ND280 site (black) is also shown.

127 scitillator by glue with glued fiber in it, cut by mill and polished to form an optical contact
 128 between the fiber end and the MPPC. Cover a) is clicked into place on ferrule b) and used
 129 to fix MPPC in optical contact. To ensure the tightness of the contact between the MPPC
 130 window and the fiber's end in ferrule a special spring made of sponge rubber is used (Fig.
 131 8). For each MPPC, 667 pixels of APD are aligned in a shape of square 1.3 mm on a side.

132 Construction of scintillator bars of the Side-MRD modules had been completed at INR
 133 in Russia, and they were transported to Japan in July 2017. Before and after the shipping
 134 their perfomance were check with cosmic rays. The main mesured parameters were light
 135 yield and light yield assymetry. For the light yields LY_1 and LY_2 at counter's two ends
 136 correspondent assymetry is calculated as $100\% \times \frac{LY_1 - LY_2}{LY_1 + LY_2}$. Thus at INR we selected 324
 137 counters from total 332 produced with mean light yield of 45 p.e./MIP and assymetry less
 138 than 10 % at the center of the bar. When counters arrived to Japan their perfomance were
 139 checked once again at Yokohama National University. In the bench setup here two small
 140 trigger counters were put in the center of measured bars. Trigger signal is the coincidence
 141 between top and bottom trigger counters made of $NaI(Tl)$ crystals of $6 \times 6 \times 17 cm^3$ size.
 142 Average total light yield obtained in the central part of the scintillator slab is 40 p.e./MIP
 143 and varies from 32 to 50 p.e./MIP. (Fig. 9 (left)). Only two counters here showed relatively
 144 high assymetry close to 25 % as shown in Fig. 9 (right). By such quality assurance tests of
 145 the counters we selected 320 scintillator bars to be installed in four Side-MRD modules. In
 146 addition, for four counters there were measured time resolution for single and combination
 147 of the counters. For one counter time resolution defined as uncertanty on $(T_{left} - T_{right})/2$

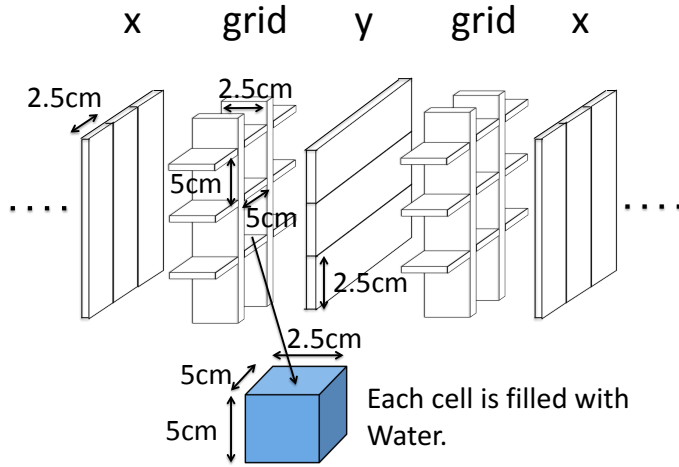


Figure 4: Schematic view of 3D grid-like structure of plastic scintillator bars inside the central detector.

¹⁴⁸ was obtained $\sigma = 1\text{ns}$ (Upper left plot in Fig. 10). Further, for a set of n counters combined
¹⁴⁹ time resolution will be $\frac{(T_L-T_R)_1+(T_L-T_R)_2+\dots+(T_L-T_R)_n}{2\times n}$. The result of combination of 2,3,4
¹⁵⁰ counters is 0.79 ns, 0.66 ns and 0.68 ns accordingly (Fig. 10).

¹⁵¹ Construction of Side-MRD modules will be done from November 2017 to January 2018
¹⁵² at Yokohama National University, then they will be transported to J-PARC and will be
¹⁵³ installed to the B2 floor of the T2K near detector hall before staring the T2K beam in
¹⁵⁴ March 2018.

¹⁵⁵ 3 Physics goals

¹⁵⁶ We will measure the differential cross section for the charged current interaction on H_2O
¹⁵⁷ and/or CH. The water-scintillator mass ratio of the Wagasci module is as high as 5:1 and
¹⁵⁸ the high purity measurement of the cross section on H_2O is possible. One experimental
¹⁵⁹ option is to replace one of the two Wagasci module with the T2K proton module which is
¹⁶⁰ fully made with plastic scintillators. It will allow the precise comparison of cross section
¹⁶¹ between H_2O and CH and also comparison of cross sections with ND280. Another option
¹⁶² is to remove water from one of the two Wagasci module. The water-out WAGASCI module
¹⁶³ will make it possible to measure wider- angle scatterings for CH target and will provide a
¹⁶⁴ low density medium for the detection of low momentum protons. The water-out WAGASCI
¹⁶⁵ data also can be used to subtract the background from interaction with scintillators in the
¹⁶⁶ water target measurement . Our setup would allow the measuemrents of inclusive and

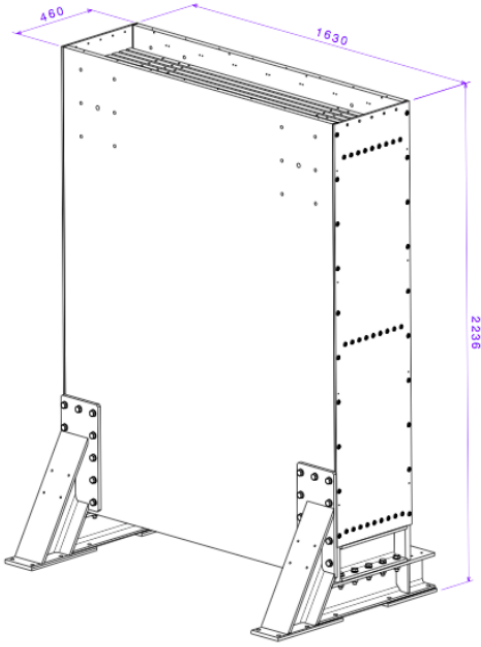


Figure 5: Support structure of the Side-MRD module.

167 also exclusive channels such as $1-\mu$, $1-\mu 1p$, $1-\mu 1\pi \pm np$ samples, former two of which are
 168 mainly caused by the quasi-elastic and $2p2h$ interaction and the latter is mainly caused by
 169 resonant or coherent pion production and deep elastic scattering. In general, an accelerator
 170 produced neutrino beam spectrum is wide and the energy reconstruction somehow rely on
 171 the neutrino interaction model. Therefore, recent neutrino cross section measurement
 172 results including T2K are given as a flux-integrated cross section rather than cross sections
 173 as a function of the neutrino energy to avoid the model dependency. We can provide
 174 the flux-averaged cross section. In addition, by combining our measurements with those at
 175 ND280, model-independent extraction of the cross section for narrow energy region becomes
 176 possible. This method was demonstrated in ?? and also proposed by P** (NUPRISM).
 177 add Yasutome plot here or later.

178 3.1 Expected number of events

179 Expected number of neutrino events after the event selections is evaluated with Monte
 180 Carlo simulations as we will discuss in Section 6. 2.41×10^4 CC events are expected in
 181 two WAGASCI modules after the selection with 1×10^{20} POT in neutrino-mode, and its
 182 purity is 75.5 %. In case we choose the option with one WAGASCI module and the T2K

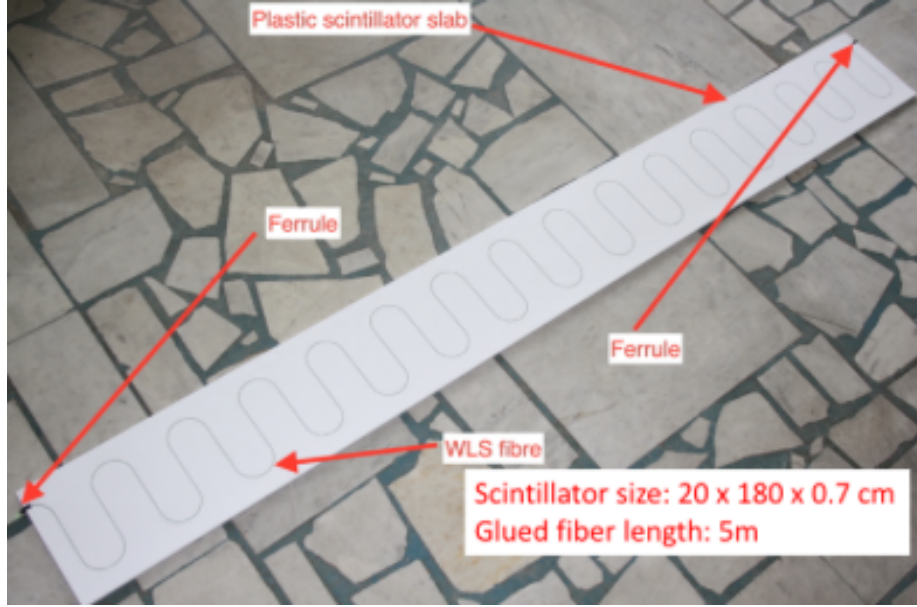


Figure 6: Scintillator bar of the Side-MRD modules.

183 proton module, 1.2×10^4 CC events are expected in the WAGASCI module and $\sim 1 \times 10^4$
 184 CC events are expected in the T2K proton module. In case we choose the option with one
 185 water-in WAGASCI module and one water-out WAGASCI module, 1.2×10^4 CC events are
 186 expected in the water-in module and 0.24×10^4 CC events are expected in the water-out
 187 module.

188 3.2 Nuclear effects

189 In T2K experiment, neutrinos interact with bound nucleons in relatively heavy nuclei
 190 (Carbon and Oxygen), so the cross-section is largely affected by nuclear effects. The nuclear
 191 effects are categorized as nucleons' momentum distribution in nucleus, interactions with
 192 correlated pairs of nucleons in nucleus (two particles-two holes, 2p2h), collective nuclear
 193 effects calculated with Random Phase Approximation (RPA) and final state interactions
 194 (FSI) of secondary particles in the nuclei after the initial neutrino interactions.

195 The 2p2h interactions mainly happen through Δ resonance interactions following a
 196 pion-less decay and interactions with a correlated nucleon pair. The 2p2h interactions are
 197 observed in electron scattering experiments (add ref. here) where the 2p2h events observed
 198 in the gap between Quasi-Elastic region and Pion-production region as shown in Fig. ??.

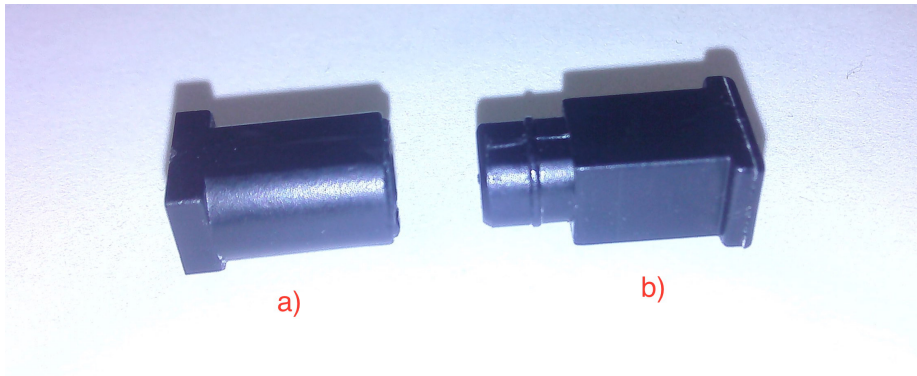


Figure 7: Optical connector for the Side-MRD scintillator. a) MPPC cover. b) Ferrule.

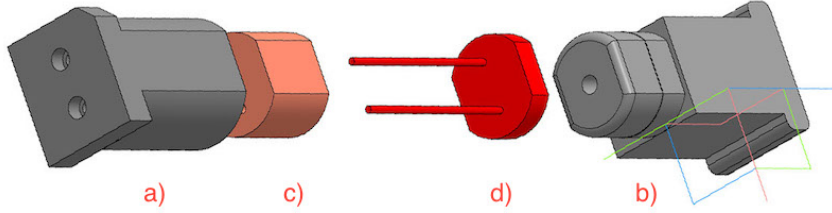


Figure 8: Scheme of the MPPC placement in optical connector. a) MPPC cover. b) Ferrule. c) Spring (sponge rubber). d) MPPC.

199 Neutrino experiments also attempt to measure the 2p2h interactions, but separation of the
 200 QE peak and the 2p2h peak is more difficult because transferred momentum (p) and energy
 201 (w) are largely affected by neutrino energies which cannot be determined event-by-event in
 202 the wide energy spectrum of the accelerator neutrino beam. Our model-independent narrow
 203 neutrino spectra extracted from combined analyses of our data and ND280 data are ideal
 204 for searching the 2p2h interaction because clearer separation of the QE peak and the 2p2h
 205 peak is expected. Another way to observe the 2p2h interaction is direct measurement of
 206 proton tracks in CC 0π sample with low detection threshold and full acceptance. Fig. ??
 207 shows proton multiplicities in CCQE events and 2p2h events, and Fig. ?? shows opening
 208 angles among two proton tracks in the same samples. The water-out WAGASCI can provide
 209 good sample for the 2p2h interaction search because its low density medium enables the
 210 detection of low momentum protons in addition to the full acceptance.

211 The corrections from collective nuclear effects calculated by RPA as a function of Q^2 are
 212 shown in Fig. ?? . The Q^2 dependence of the correction can be tested by measuring angular

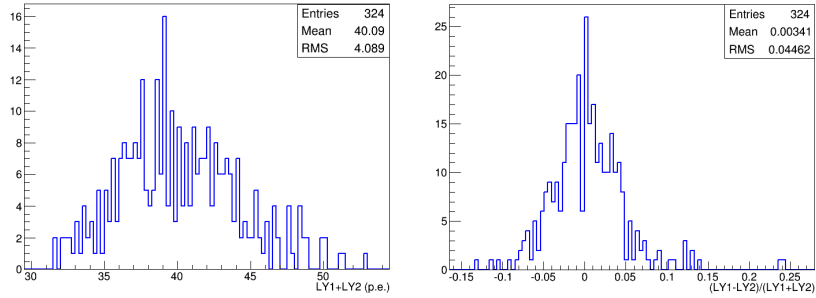


Figure 9: Total light yield distribution (left) and light yield assymetry (right) measured at YNU.

213 distribution of muons in CC1- μ and CC1- $\mu 1p$ events. The uncertainties of the corrections
 214 in low (high) Q^2 regions can be constrained by observing the events with a forward-going
 215 (high-angle) muon, so it is essential to measure muon tracks with full acceptance.

216 T2K experiment is starting to use ν_e CC1 π events for its CP violation search to increase
 217 the statistics. One of the biggest uncertainty of the CC1 π sample comes from the final
 218 state interactions of pions in the nuclei after the initial neutrino interactions because they
 219 change the multiplicity, charge and kinematics of the pions. The multi-pion production
 220 events can be migrated into the CC1 π sample due to the FSIs, and they become important
 221 backgrounds. We can constrain the uncertainties from the pion FSIs by measuring pion
 222 rescattering in the detector and pion multiplicity in ν_μ CCn π sample with low detection
 223 threshold and full acceptance for pion tracks. The water-out WAGASCI can provide good
 224 sample for the pion FSI studies because its low density medium enables the detection of
 225 low momentum pions in addition to the full acceptance.

226 4 Status of J-PARC T59 experiment

227 We had submitted a proposal of a test experiment to test a new detector with a water
 228 target, WAGASCI, at the T2K near detector hall to J-PARC PAC on April 2014, and the
 229 proposal was approved as J-PARC T59. There are several updates on the project after
 230 three years from then. Fist, the start time of neutrino beam measurement is changed from
 231 December 2015 to October 2017, and the requested neutrino beam is changed from 1×10^{21}
 232 POT of ν beam to 0.8×10^{21} POT of anti- ν beam. Second, the detector configuration is
 233 changed. In the original proposal, central neutrino detector are expected to be surrounded
 234 by newly developed muon-range detectors (MRDs), but we will use spare neutrino detectors
 235 of the T2K experiment instead of them during neutrino beam measurement from October
 236 to December 2017. Construction of the newly developed MRDs, Baby-MIND and Side-

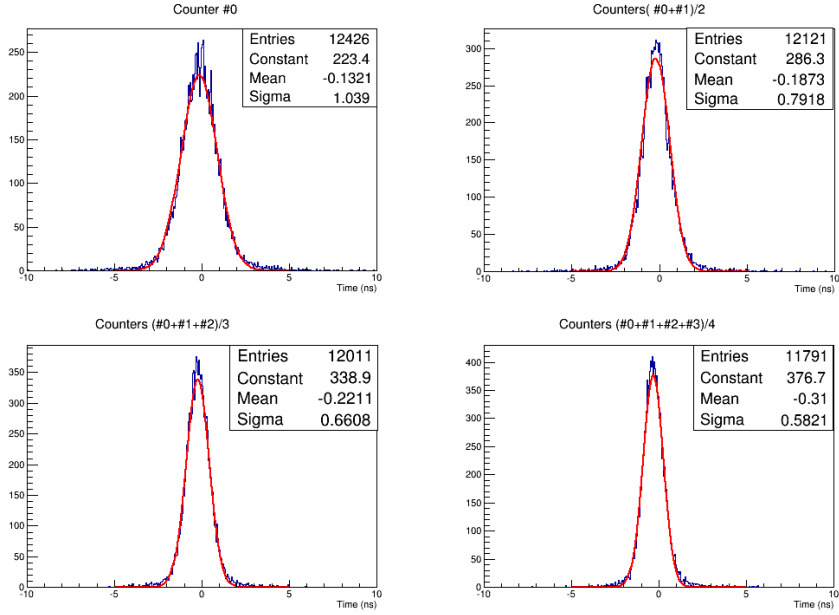


Figure 10: Time resolution for one (upper left) and a set of 2,3,4 Side-MRD counters.

237 MRD, is in progress, and they will be installed to the both sides and the downstream of
 238 the central neutrino detector from January to March 2018. Then, we will resume neutrino
 239 beam measurements from March 2018 and will take the neutrino beam data until May
 240 2018.

241 4.1 On-axis beam measurement with Prototype detector

242 Add INGRID water module measurement here.

243 4.2 Plans from October 2017 to May 2018

244 J-PARC MR will extract its proton beam to T2K neutrino beam-line from October to
 245 December 2017, and, from March to May 2018. T2K experiment will produce anti-neutrino
 246 beam and will accumulate $\sim 8 \times 10^{20}$ POT data during the above period.

247 J-PARC T59 will perform neutrino beam measurements on the B2 floor of the T2K
 248 near neutrino detector hall during the above period to test basic performances of the
 249 WAGASCI detector and new electronics. During the beam measurements from October to
 250 December 2017, one WAGASCI module will be placed between spare neutrino detectors of
 251 the T2K experiment, INGRID Proton module and INGRID standard module. Here, the
 252 INGRID Proton module is used as a charged particle VETO detector and, the INGRID

253 standard module is used as a downstream muon detector. We had submitted a proposal
254 to use these spare neutrino detectors for the T59 neutrino beam measurements to the T2K
255 collaboration, and we got an approval from T2K.

256 During the beam measurements from March to May 2018, Baby-MIND and two side
257 muon-range detector (Side-MRD) modules will be installed on the downstream and the
258 both sides of the WAGASCI detector, as shown in Fig. 11, to increase angular acceptance
259 for secondary charged particles from neutrino interactions. Add Baby-MIND commissioning
260 items here!!!

tmp.pdf

Figure 11: J-PARC T59 detector configuration with Baby-MIND and two Side-MRD modules from Mar. to May 2018. (Need to prepare the figure.)

261 Expected number of neutrino events in the WAGASCI detector during the above beam
262 period is evaluated with Monte Carlo simulations. Neutrino beam flux at the detector
263 location is simulated by T2K neutrino flux generator, JNUBEAM, neutrino interactions
264 with target materials are simulated by a neutrino interaction simulator, NEUT, detector
265 responses are simulated using GEANT4-based simulation. The neutrino flux at the detector
266 location, 1.5 degrees away from the J-PARC neutrino beam axis, is shown in Figure 3, and
267 its mean neutrino energy is around 0.68 GeV. An event display of the GEANT4-based
268 detector simulation is shown in Figure 14.

269 To perform the detector performance test, the following event selections are applied to
270 the data. First, track reconstructions are performed in the WAGASCI detector, and the
271 reconstructed vertex is required to be inside a defined fiducial volume, $80 \times 80 \times 32 \text{ cm}^3$
272 region at the center of the detector, to reduce contamination from external backgrounds.
273 Second, at least one charged particle is required to reach to INGRID standard module

274 or Side-MRD modules, and it makes more than two hits in these sub-detectors. With the
275 event selection, expected numbers of the neutrino-candidate events during the beam period
276 are summarized in Table 1. Using the data, we will test the detector performance with
277 $\sim 3\%$ statistical uncertainties.

278 5 Detector performance

279 5.1 Wagasci module

280 To demonstrate the performance of the Wagasci module and also to study the neutrino
281 interaction, the first Wagasci module was installed at the on-axis position, in front of
282 the T2K INGRID horizontal center module in 2016. The INGRID module is made of iron
283 plates and segmented plastic scintillator bars. It's cross sectional size viewed from the beam
284 direction is $1 \text{ m} \times 1 \text{ m}$. The charged current interactions in the Wagasci module are selected
285 by requiring a muon track candidate in the INGRIRD modules. Here, we describe the
286 performance of the Wagasci module evaluated at this T2K on-axis measurement. Figure 12
287 shows the light yeild of channels for muons produced by the interaction of neutrinos in the
hall wall. The light yield is sufficiently hgih to get good hit efficieincy. A track search

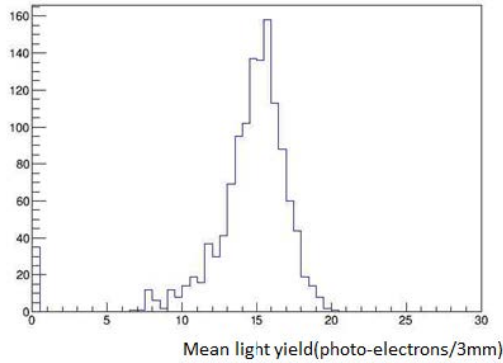


Figure 12: Light yield of channels for muons produced by the interaction of neutrinos in the hall wall.

288 algorithm based on the cellular automaton has been developed using the software tools by
289 the T2K INGRID. The tracking efficiency in 2-dimentional projected plane was evalualted
290 by comparing the reconstructed track in the Wagasci module and the INGRID module and
291 shown in Fig.13. Note that that the tracking efficinecy for high angle ($> 70 \text{ deg}$) is not
292 evaluated because of the acceptance of the INGRID module, not because of the limitation
293 of the Wagasci module.

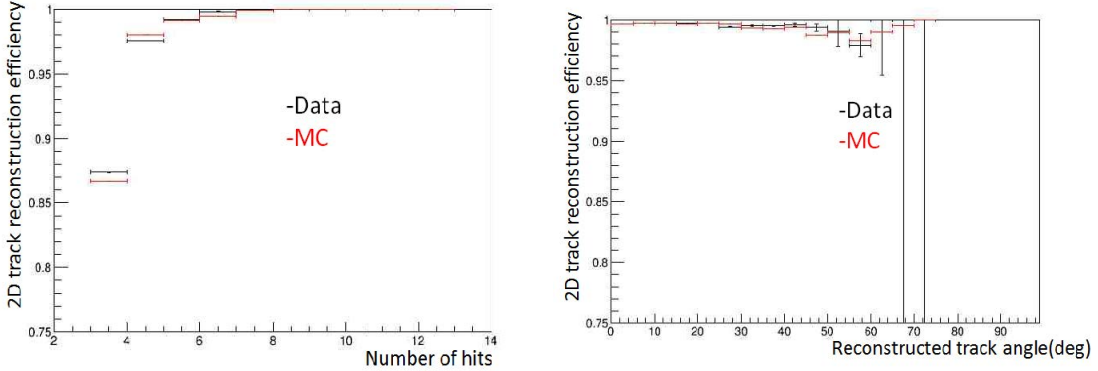


Figure 13: 2D track reconstruction efficiency as a function of number of hits (left) and track angle (right). Here the track angle is the one reconstructed by the INGRID module.

295 **5.2 Baby MIND**

296 **5.3 Side muon range detector**

297 **6 MC studies**

298 **6.1 Detector simulation**

299 Expected number of neutrino events in the WAGASCI detector is evaluated with Monte
300 Carlo simulations. Neutrino beam flux at the detector location is simulated by T2K neutrino
301 flux generator, JNUBEAM, neutrino interactions with target materials are simu-
302 lated by a neutrino interaction simulator, NEUT, detector responses are simulated using
303 GEANT4-based simulation. The neutrino flux at the detector location, 1.5 degrees away
304 from the J-PARC neutrino beam axis, is shown in Figure 3, and its mean neutrino energy
305 is around 0.68 GeV.

306 **6.1.1 Detector geometry**

307 The detector geometry in the GEANT4-based simulation is slightly different from the
308 actual detector as shown in Fig. 16. The active neutrino target region consists of four
309 WAGASCI modules, and each WAGASCI detector has the dimension with 100 cm \times 100
310 cm in the x and y directions and 50 cm along the beam direction. An event display of a
311 MC event in the WAGASCI detectors is shown in Figure ???. Two Side-MRD modules is
312 installed at both sides of the WAGASCI modules, and each Side-MRD module consists of
313 ten iron plates whose dimension is 3 cm (thickness) \times 180 cm (height) \times 320 cm (width).
314 The distance between the Side-MRD modules and WAGASCI modules is 60 cm. The

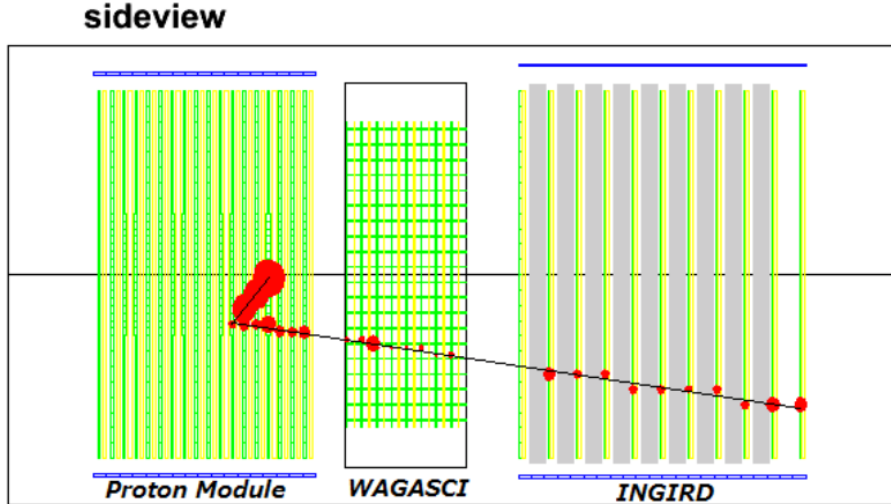


Figure 14: J-PARC T59 event display of a neutrino event in the GENAT4-based detector simulation.

315 downstream-MRD equivalent to the Baby-MIND is installed at the downstream of the
 316 WAGASCI modules. The downstream-MRD consists of ten iron plates whose dimension is
 317 3 cm (thickness) \times 180 cm (height) \times 320 cm (width) and another ten iron plates whose
 318 dimension is 6 cm (thickness) \times 180 cm (height) \times 320 cm (width). The distance between
 319 the downstream-MRD modules and WAGASCI modules is 60 cm.

320 In order to estimate backgrounds from neutrino interactions in the wall and floor of the
 321 experimental hall, the geometry of the experimental hall is implemented in the GEANT4-
 322 based detector simulation.

323 **6.1.2 Response of detector components**

324 The energy deposit inside the scintillator is converted into the number of photons. The
 325 effects of collection and attenuation of the light in the scintillator and the WLS fiber are
 326 simulated, and the MPPC response is also taken into account. The light yield is smeared
 327 according to statistical fluctuations and electrical noise.

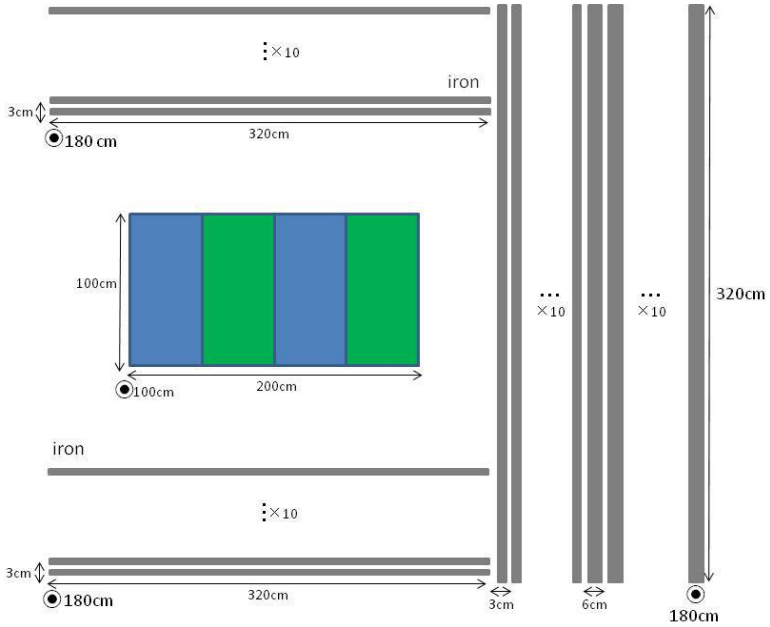


Figure 15: Geometry of the detectors in the Monte Carlo simulation.

328 6.2 Track reconstruction

329 To select neutrino interaction from the hit patterns, a track reconstruction algorithm is
 330 developed. The flow of the track reconstruction is as follows.

- 331 1. Two-dimensional track reconstruction in each sub-detectors
 - 332 2. Track matching among the sub-detectors
 - 333 3. Three -dimensional track reconstruction
- 334 Add explanation about two-dim reco, track matching and three-dim reco here.

335 6.3 Event selection

336 The events with the track which starts in 5 cm from the wall of the WAGASCI module are
 337 rejected to remove the background from the outside as shown in Fig. 17.

338 To reject backgrounds from NC and neutral particles, the longest tracks are required to
 339 penetrate more than one (five) iron plates in Side-MRD modules (Baby-MIND) as shown
 340 in Figure 18. In order to measure muon momentum, the longest tracks are required to stop
 341 in MRDs (Side-MRD modules and Baby-MIND) or penetrate all iron plates.

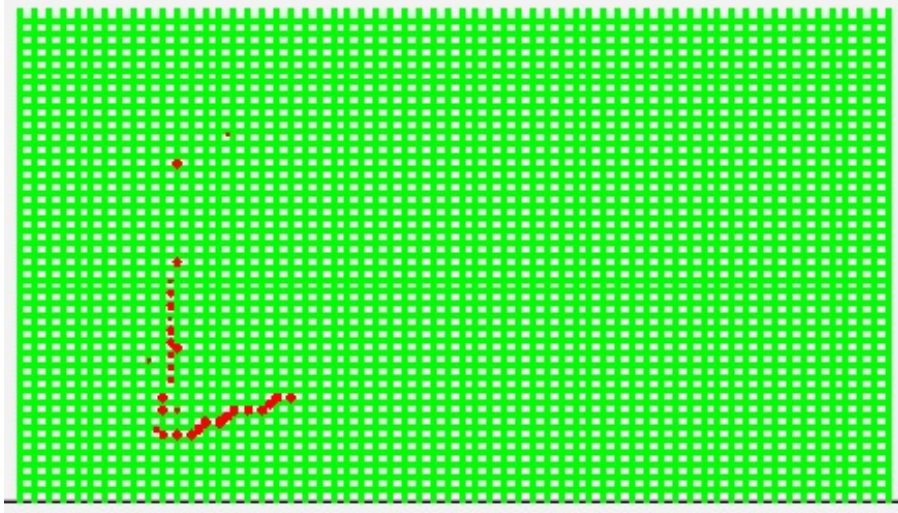


Figure 16: An event display of MC event in WAGASCI detectors. Green lines are scintillators and red circles are the hit channels.

342 6.4 Selected events

343 Table 1 shows numbers of the selected events after each event election. 2.41×10^4 CC events
344 are expected with 1×10^{21} POT in neutrino-mode, and the purity is 75.5 %. The main
345 background is the neutrino interaction in the scintillators inside the WAGASCI detector.

Table 1: Expected number of the neutrino-candidate events in two WAGASCI modules after the event selections with 1×10^{21} POT in neutrino-mode.

Cut	CC	NC	BG (Scinti.)	BG (outside)	
Track reconst.	6.27×10^4	3.61×10^3	1.62×10^4	1.04×10^6	1.12×10^6
Fiducial	3.95×10^4	1.75×10^3	9.71×10^3	7.32×10^3	5.55×10^4
Penetrated iron	3.02×10^4	9.12×10^2	7.67×10^3	2.04×10^3	4.00×10^4
Stop in MRDs	2.41×10^4	8.65×10^2	6.19×10^3	1.64×10^3	3.19×10^4
after all cuts	75.5 %	2.71 %	19.4 %	5.14 %	100 %

346 Figure 19 shows the reconstructed angles of the longest tracks in the selected events.
347 Figure 20 shows differences between true angles and the reconstructed angles of the longest
348 tracks in the selected events, and the angle resolution is ~ 3 degrees.

349 Figure 21 shows the iron plane numbers corresponding to the end points of the longest
350 tracks in the selected events.

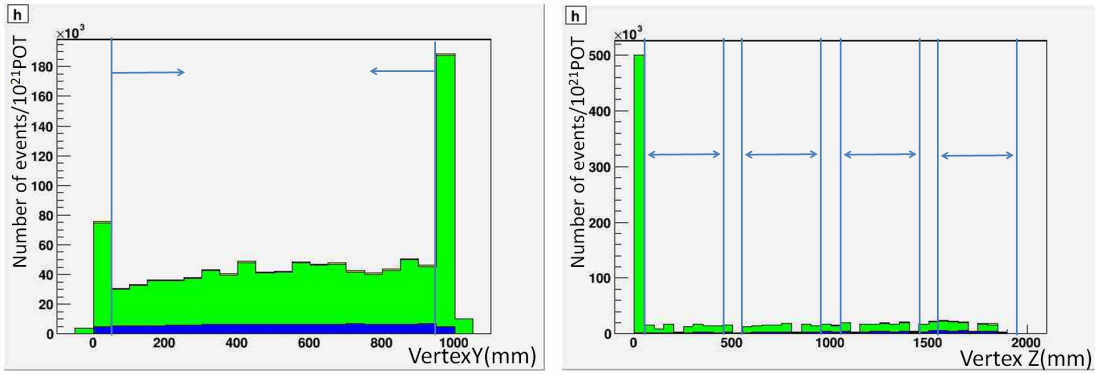


Figure 17: Event selection with the vertex of the track. Blue hist. are events from the WAGASCI modules, green hist. are events from the experimental hall, and yellow hist. are events from the Side-MRD modules and the downstream-MRD.

351 Table 2 shows particles which produce the longest tracks in the selected events, and
 352 the fraction of muons is 85.6%.

Table 2: Particles which produce the longest tracks in the selected events.

particles	fraction
μ	85.6%
π^+, π^-	4.8%
p	4.3%
e^+, e^-	4.5%

353 Figure 22 shows detection efficiencies of muon tracks in the selected events as a function
 354 of muon's true angle and true momentum. The efficiency in the large angle region is low
 355 because Side-MRD modules only cover sides of the WAGASCI modules. The efficiency in
 356 the low momentum region is also low because more than two hits are required to reconstruct
 357 the track in the WAGASCI detector.

358 6.5 Cross section measurements on water

359 In the water target events, the background from interaction with scintillators has to be
 360 subtracted by using the measurement of the hydrocarbon target.

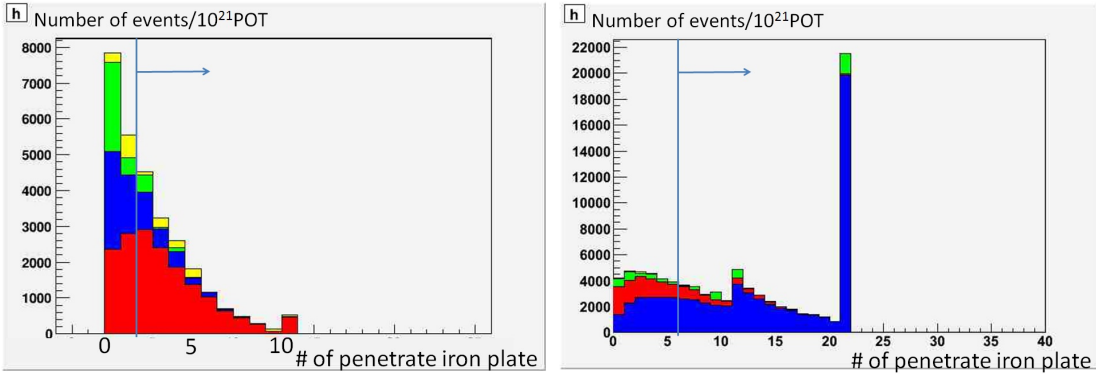


Figure 18: Event selection with the number of the penetrated iron plates in the Side-MRD modules (left) and the Baby-MIIND (right). Blue and red hist. are events from the WAGASCI modules, green hist. are events from the experimental hall, and yellow hist. are events from the Side-MRD modules and the Baby-MIIND.

361 **6.5.1 Charged current cross section measurement**

362 **7 Standalone WAGASCI-module performances**

363 In the previous sections, the WAGASCI detector was studied using the Muon Range Detectors. In this section, the standalone abilities of WAGASCI module are presented. Using
 364 the WAGASCI configuration presented in Section 6, we have evaluated that only 7% of
 365 the muons will be stopped in one of the WAGASCI modules. THowever, this proportion
 366 increases to 53% for pions and 73% for protons produced by neutrino interactions at 1.5°
 367 off-axis. Figure 23 shows the momentum distribution of these daughter particles as well as
 368 for the sub-sample stopped in one of the WAGASCI modules. Therefore, the study of the
 369 standalone abilities of the WAGASCI module in this section are dominantly motivated by:
 370

- 371 • the accurate measurement of the neutrino interaction final states. Though most of the
 372 muons will be reconstructed and identified in the MRDs, the hadronic particles will
 373 predominantly stops in one WAGASCI module. One has therefore to rely exclusively
 374 on the WAGASCI module information alone to reconstruct, identify and measure the
 375 momentum of pions or protons.
- 376 • the coverage of the MRDs is not 4π . Using the WAGASCI module information can
 377 therefore help to constraint the particles that exits the WAGASCI module but do
 378 not geometrically enters any MRD.
- 379 • the particle identification of low momenta muons $p_\mu < 300$ MeV/c that will leave only
 380 few hits in the MRD. Using the WAGASCI module information will clearly enhance

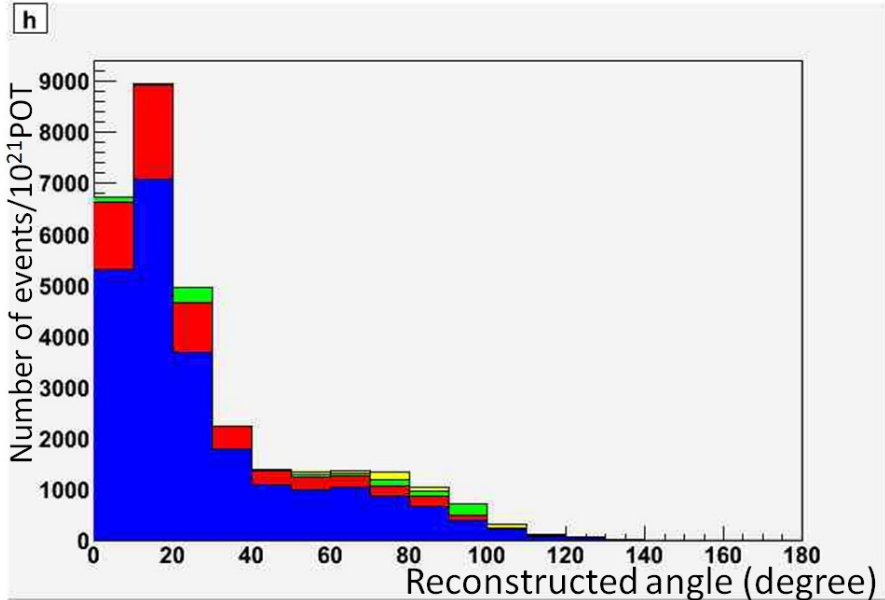


Figure 19: The reconstructed angles of the longest tracks in the selected events. Blue and red hist. are events from water and scintillators in the WAGASCI modules, green hist. are events from the experimental hall, and yellow hist. are events from the Side-MRD modules and the Baby-MIND.

381 the particle identification.

382 This study is based on an original study done for the ND280 upgrade target, with some
 383 modifications. Though the cell size is similar to the WAGASCI configuration presented
 384 in Section 6, the external dimensions are different ($186.4 \times 60 \times 130 \text{ cm}^3$). Whenever the
 385 results are presented with this external size and this parameter is likely to impact the
 386 result, it will be mentioned.

387 Note that in this section, a simplified reconstruction algorithm presented in Section 7.1 is
 388 used. The fiducial volume is chosen accordingly as the inner cube of the module which
 389 surfaces are distant of $4 \times$ scintillator space = 10 cm from the module external surfaces.

390 The neutrino interactions are simulated using NEUT v5.3.2. The NEUT input neutrino
 391 flux is estimated using JnuBeam v13a and assuming the detector to be located at 1.5°
 392 off-axis, as in Section 6. Note that the event reconstruction efficiency as a function of true
 393 neutrino energy might be changed at 1.5° , due for example to different Q^2 distributions. For
 394 this reason, one has to note that the reconstruction results might slightly be changed from
 395 2.5° and 1.5° . To avoid a similar change on the particle-only reconstruction efficiencies,
 396 they will be presented as a function of variables that completely characterize the particle

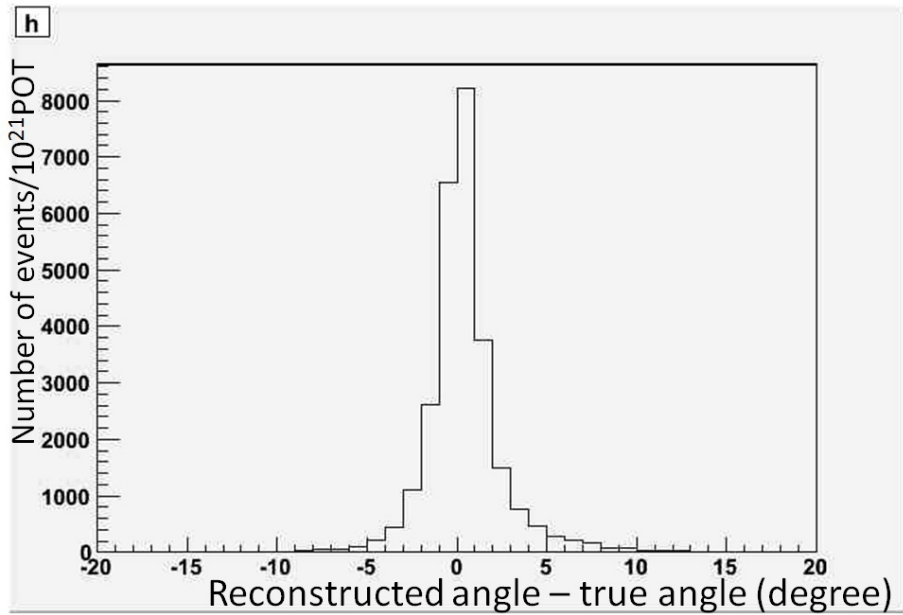


Figure 20: Differences between true angles and the reconstructed angles of the longest tracks in the selected events.

397 kinematic state, *i.e.* its momentum and angle. Figure 24 shows the vertices distributions
 398 of the daughter particles of neutrinos interacting one standard WAGASCI water-module.
 399 In this section, we will show the detector reconstruction and particle identification in this
 400 phase space, both for leptonic and hadronic particles. We will finally show an empty
 401 WAGASCI module can highly enhance the ability to constrain the neutrino interaction
 402 final state which is critical to reduce the corresponding uncertainties.

403 **7.1 Reconstruction algorithm**

404 **7.1.1 Description**

405 For this section, an ideal “simulated” reconstruction is developed. A particle is recon-
 406 structed if:

- 407 1. The particle is charged.
 408 2. Lets at least one hit (energy deposit > 2.5 photo-electron) in a scintillator.
 409
 410 3. The particle enters one TPC and let one hit in the tracker.
 411 Or

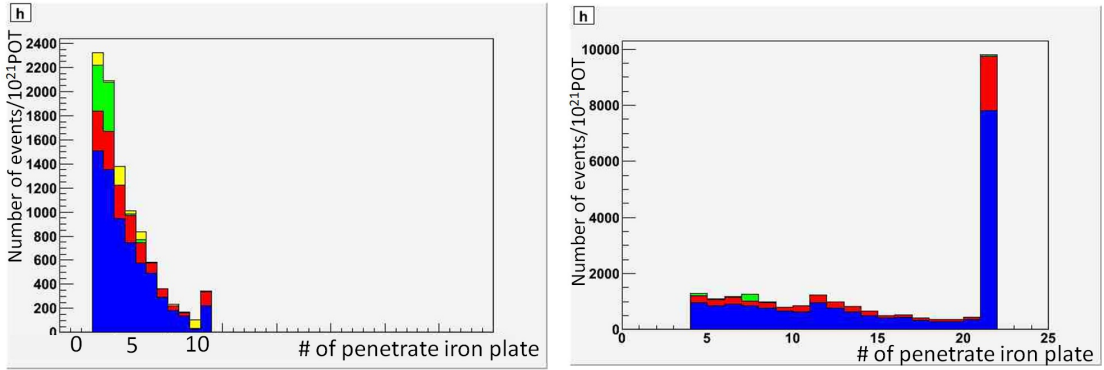


Figure 21: Iron plane numbers in Side-MRD (left) and Baby-MIND (right) corresponding to the end points of the longest tracks in the selected events. Blue and red hist. are events from water and scintillators in the WAGASCI modules, green hist. are events from the experimental hall, and yellow hist. are events from the Side-MRD modules and the Baby-MIND.

412

413

- The particle should be long enough to be reconstructed by the detector in at least 2 out of 3 views (XZ, YZ, XY). The length criterion requires the particle to let at least 4 hits in the detector. In the “less favourable case” of pure longitudinal or transverse going tracks, it represents a the track length of $L_{track} \geq 4 \times$ scintillator space = 10.0 cm.
- In the views where particles pass the length criterion, the particle shall not be superimposed with longer tracks in at least two views. The superposition criterion is estimated with the distance inter-tracks (DIT) which corresponds to the orthogonal distance between two tracks at the ending point of the shortest one (see Figure 25). For a track 1, the superposition criterion is tested with every longer tracks that starts at the same vertex. Let \vec{p}_1 the vector of track 1, and p_1^a its projections in the XZ, YZ and XY planes respectively for $i=1,2,3$. Note that these are projections in a 2D planes and not on a direction vector. In this case, the relative angle between the track 1 and a longer track 2 (of vector \vec{p}_2) in a view a is given by:

$$\cos \theta = \frac{\vec{p}_1^a \cdot \vec{p}_2^a}{\|\vec{p}_1^a\| \|\vec{p}_2^a\|} \quad (1)$$

428

and the distance inter track is given by:

$$DIT = \|\vec{p}_1^a\| \sin \theta \quad (2)$$

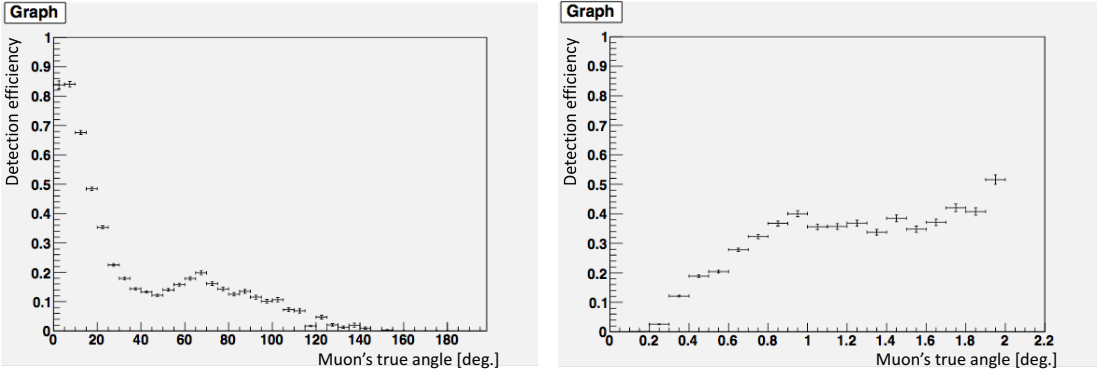


Figure 22: Detection efficiencies of muon tracks in the selected events as a function of muon's true angle (left) and true momentum (right).

429 The DIT should be higher than $4 \times$ scintillator width for the track 1 to be not
 430 superimposed with the track 2 in the view a, which also corresponds to 10.0 cm
 431 in the nominal configuration.

432 7.1.2 Performances

433 The particle-only reconstruction efficiencies and the reconstruction threshold in momenta
 434 are shown in Table 3. This threshold is defined as the maximal momentum for which the
 435 reconstruction efficiency is smaller than 30%. The thresholds in muon and pion momenta
 436 are 150 MeV/c. Most of the muons are above this threshold (see Figure 24) which leads
 437 to a 79% reconstruction efficiency.

	μ	π	p
Reconstruction Efficiency	79%	52%	26%
Momentum threshold	150 MeV/c	150 MeV/c	550 MeV/c

Table 3: Reconstruction efficiency and momentum threshold for muons, pions and protons. The threshold is defined as the maximal momentum for which particles have a reconstruction efficiency smaller than 30%.

438 The lower pion and proton efficiencies (respectively 52% and 26%) are due to lower
 439 efficiencies for similar momenta than muons, coming from strong interactions as shown
 440 on Figures 26. Efficiencies of each particle type tend to decrease in the backward region

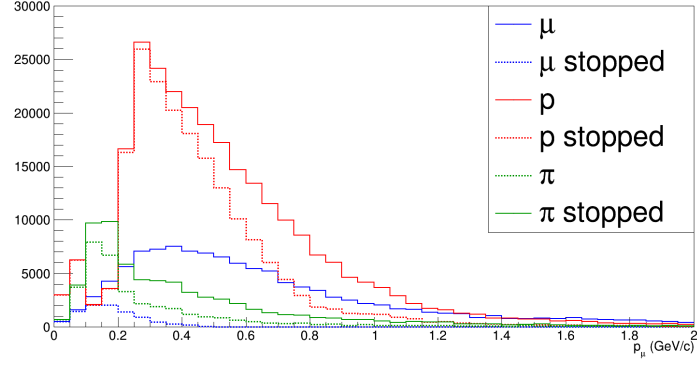


Figure 23: Momentum distribution of true particles in WAGASCI (plain) and corresponding distributions only for particles stopping into the WAGASCI module (dashed).

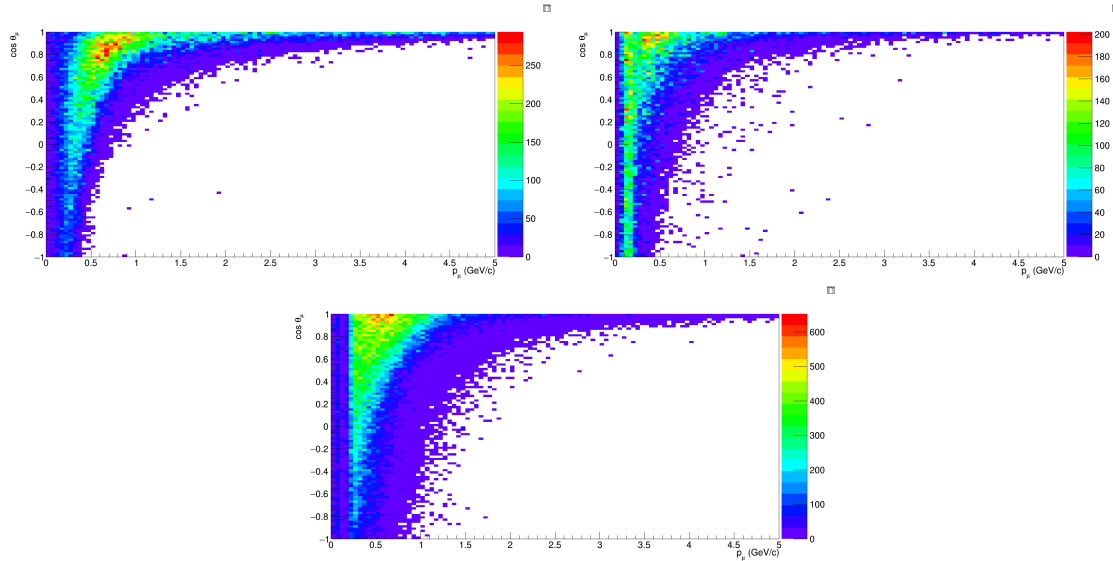


Figure 24: True number of muons (left), charged pions (right) and protons (bottom) in the two WAGASCI water-module as a function of the particles momenta and angles at 1.5° .

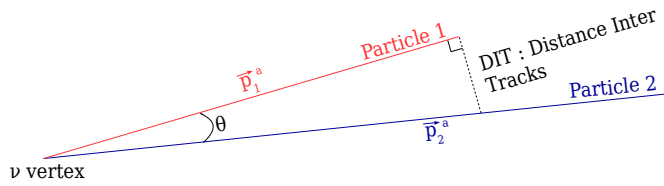


Figure 25: Definition of the distance inter tracks.

⁴⁴¹ due to particle lower momenta. However, for a fixed momentum value, the reconstruction
⁴⁴² efficiency is almost uniform which confirms the ability of the WAGASCI detector to
⁴⁴³ reconstruct high angle tracks.

⁴⁴⁴ The reconstruction is thereafter tested on neutrino events. Table 4 summarizes the
⁴⁴⁵ number of reconstructed events and efficiencies for each interaction type. As expected
⁴⁴⁶ from the high muon reconstruction efficiency, the charged current interactions have recon-
 struction efficiencies $\geq 85\%$.

	CC0π	CC1π	CCOthers	NC	All
Reconstruction efficiency	85%	87%	91%	22%	68%

Table 4: Number of true interactions reconstructed. The purity and reconstruction effi-
 ciency of each true interaction is also shown.

⁴⁴⁷
⁴⁴⁸ The reconstruction efficiencies as a function of the neutrino energy and muon kinematics
⁴⁴⁹ are respectively shown on Figure 27 and 28.

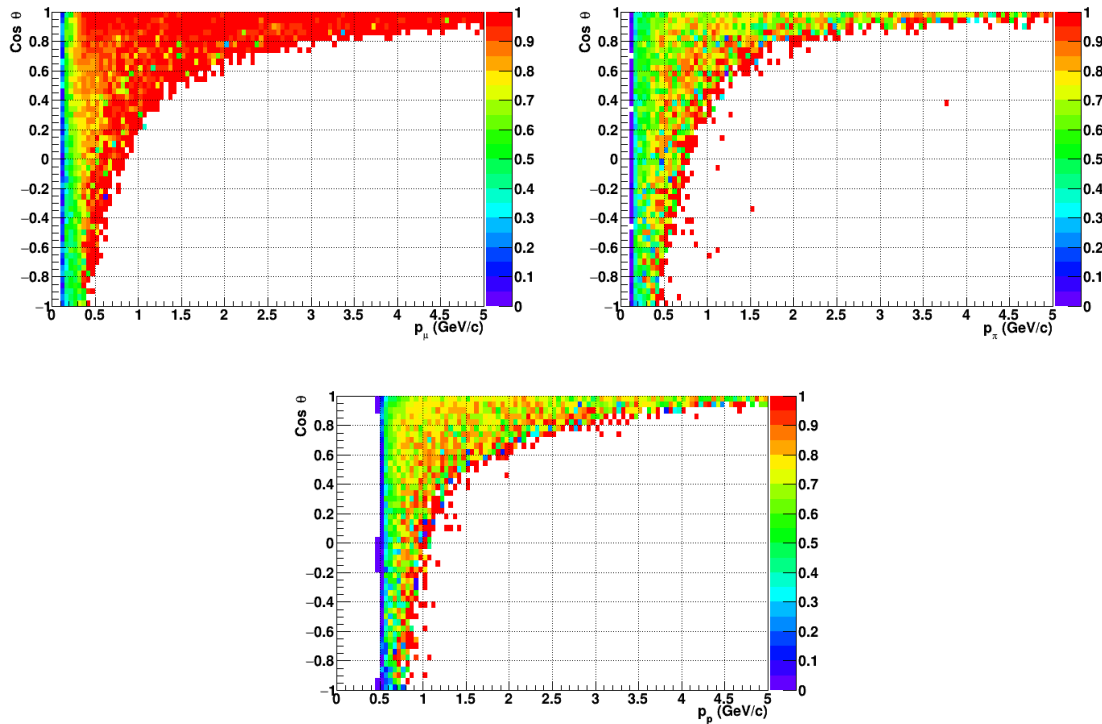


Figure 26: Reconstruction efficiency of muons (left), charged pions (right) and protons (bottom) in the WAGASCI water-module as a function of the particles momenta and angles.

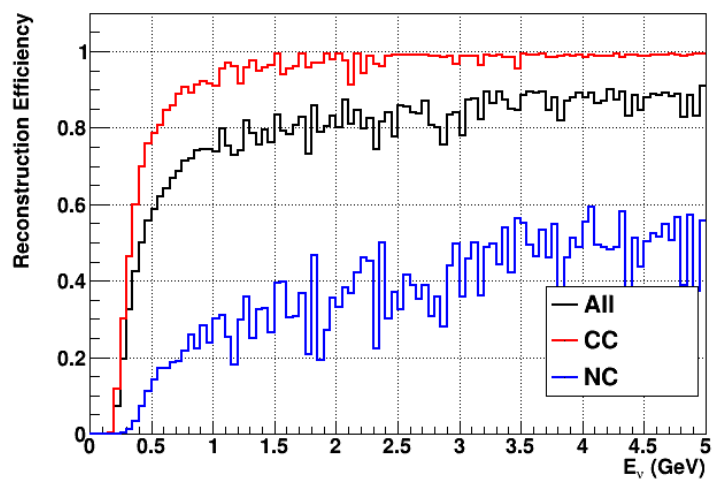


Figure 27: Reconstruction efficiency of all neutrino (black), CC (red) and NC (blue) interactions in the WAGASCI water-module as a function of the neutrino energy.

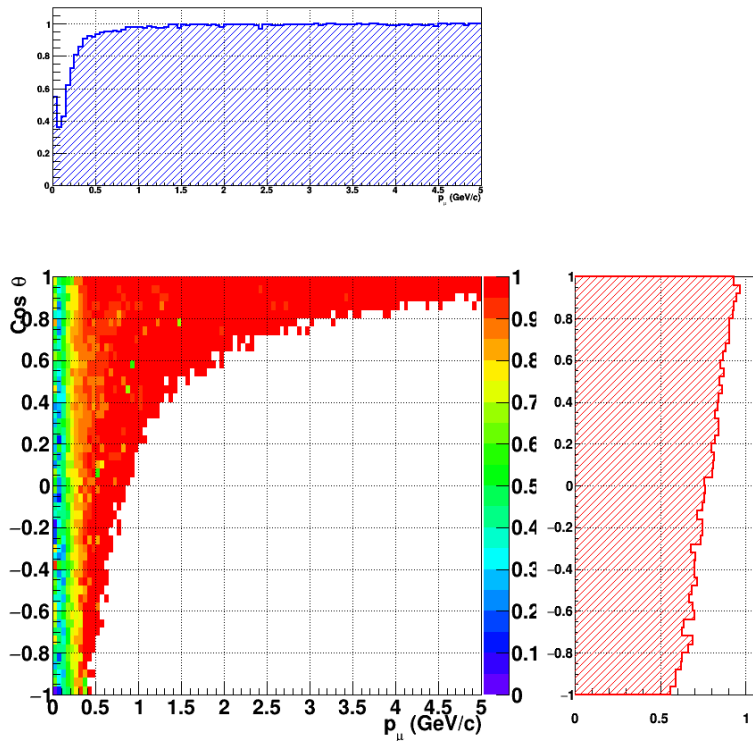


Figure 28: Reconstruction efficiency of CC interactions in the WAGASCI water-module as a function of the muon kinematic variables (momentum and angle).

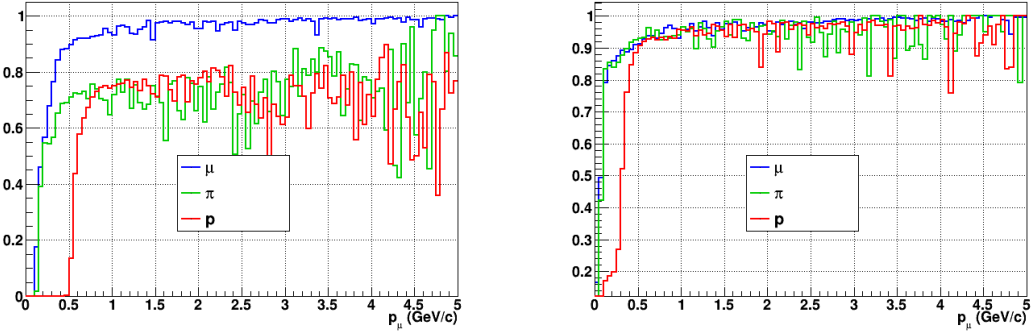


Figure 29: Reconstruction efficiency for muons, pions and protons in the water-in (left) and water-out (right) modules.

450 Note that a Particle Identification Algorithm has been also developed. It is based on
 451 the charge deposition of the particles in the scintillator, of the detection of a decay-electron.
 452 However, this information highly depends on the number of scintillator hit by a particle,
 453 which creates an important difference between a real WAGASCI module and the one used
 454 for the ND280-upgrade simulation. For this reason, the corresponding results will not be
 455 detailed here, but can be found in [?].

456 7.2 Background subtraction: the water-out module

457 In the nominal configuration, 20% of the neutrino interactions occurs on scintillators
 458 (C_8H_8). This background should be removed in order to measure the neutrino interac-
 459 tion on the same target as Super-K, which suppress the differences in cross-section models.
 460 For this purpose, we propose to use a water-out module, where the water is replaced by
 461 air. The detector is therefore fully active and has a 3 mm spatial resolution (scintillator
 462 thickness) which create an ideal detector to reconstruct and identify hadrons, and study
 463 np-nh interactions. The counter-part is the difference in particle energy deposition between
 464 the water and this water-out module that will need to be corrected for. In this section,
 465 we present the capabilities of such a module, and the impact it can have on cross-section
 466 measurements for the neutrino community in general and T2K in particular.
 467 The same reconstruction and selection as the water-in module is applied. Figure 29 shows
 468 the comparison between the water-in and the water-out reconstruction efficiencies for muon,
 469 pions and protons. 90% of the muons and 87% of the pions are reconstructed, while 70%
 470 of the protons are even reconstructed. It allows to lower down the proton threshold to
 471 250 MeV/c (see Table 5).

472 As a consequence of tracking even low momenta particle, the reconstruction efficiency
 473 is uniform and almost maximal on the entire $\cos \theta_\mu$ phase space, as shown on Figure 30.

	μ	π	p
Reconstruction Efficiency Momentum threshold	90% 50 MeV/c	87% 50 MeV/c	70% 250 MeV/c

Table 5: Reconstruction efficiency, proportions of μ -like and non μ -like and momentum threshold for muons, pions and protons in the empty module. The threshold is defined as the maximal momentum for which particles have a reconstruction efficiency smaller than 20%.

474 Since the fiducial mass represents 0.25 tons, the total number of events is divided by a
 475 factor of 3 compared to the water-in module. The water-out module offers interesting
 476 possibilities to study np-nh interaction since 70% of the protons are reconstructed. In the
 477 future, a possible separation as a function of the number of proton track will be studied.
 478 Moreover, we are currently pursuing the use of single and double transverse variables (cite
 479 Xianguo) to open new possibilities for separating np-nh from Final State Interactions, or
 480 for isolating the interactions on hydrogen from interactions on carbon in this module.

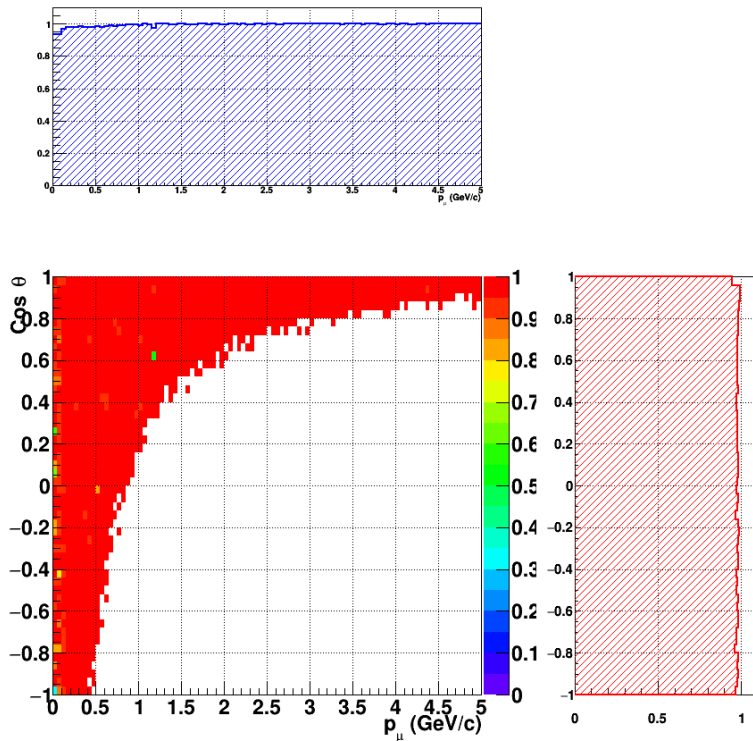


Figure 30: Reconstruction efficiency of CC interactions in the WAGASCI empty module as a function of the muon kinematic variables (momentum and angle).

481 **8 Schedule**

482 We would like to start a physics data taking from T2K beam time after the summer
483 shutdown in 2018. By then, commissioning and tests of the detectors will be completed
484 in J-PARC T59. The experiment can run parasitically with T2K, therefore we request no
485 dedicated beam time nor beam condition as discussed in the following section.

486 Once the approved POT is accumulated, the WAGASCI modules will be removed
487 from the experimental site, but we would like to keep the Baby-MIND and the Side-MRD
488 modules on the B2 floor of the NM pit as common platforms of future neutrino experiments
489 using the T2K neutrino beam.

490 **9 Requests**

491 **9.1 Neutrino beam**

492 The experiment can run parasitically with T2K, therefore we request no dedicated beam
493 time nor beam condition. As data taking periods, we request the ‘nominal’ T2K one-year
494 operation both for the neutrino beam and the antineutrino beam. The T2K has been
495 requesting 0.9×10^{21} POT/year and actually accumulating about 0.7×10^{21} POT/year in
496 recent years. For each year, starting from the Autumn, T2K is running predominantly in
497 the neutrino mode or in the antineutrino mode. Our request is to have one-year neutrino-
498 mode data and another one-year antineutrino mode data assuming that the POT for the
499 fast extraction in each year is more than 0.5×10^{21} POT.

500 **9.2 Equipment request including power line**

501 We request the followings in terms of equipment on the B2 floor:

- 502 • Site for the WAGASCI modules, Side-MRD modules and BabyMIND and their elec-
503 tronics system on the B2 floor of the near detector hall (Fig. 2).
- 504 • Anchor points (holes) on the B2 floor to secure the WAGASCI modules, Side-MRD
505 module and Baby-MIND (Fig. ??)
- 506 • Power line for the magnets in Baby-MIND: 400 V tri-phase 48-to-62 Hz, capable of
507 delivering 12 kW.
- 508 • Electricity for electronics and water circulation system, 3 kW, standard Japanese
509 electrical sockets.
 - 510 1. Online PCs: 2.1 kW
 - 511 2. Electronics: 0.7 kW
 - 512 3. Water sensors: ?

- 513 • Air conditioner for cooling heat generation at Baby-MIND magnets, online PCs and
514 electronics
- 515 • Beam timing signal and spill information
- 516 • Network connection

517 **10 Conclusion**